Petroleum Science (2020) 17:1298–1317
https://doi.org/10.1007/s12182-020-00451-z

ORIGINAL PAPER

Impact of solutal Marangoni convection on oil recovery during chemical flooding

Sepideh Palizdan[1] · Jassem Abbasi[1] · Masoud Riazi[1] · Mohammad Reza Malayeri[1]

Received: 1 November 2019 / Published online: 24 April 2020

Abstract

In this study, the impacts of solutal Marangoni phenomenon on multiphase flow in static and micromodel geometries have experimentally been studied and the interactions between oil droplet and two different alkaline solutions (i.e. $MgSO_4$ and Na_2CO_3) were investigated. The static tests revealed that the Marangoni convection exists in the presence of the alkaline and oil which should carefully be considered in porous media. In the micromodel experiments, observations showed that in the $MgSO_4$ flooding, the fluids stayed almost stationary, while in the Na_2CO_3 flooding, a spontaneous movement was detected. The changes in the distribution of fluids showed that the circular movement of fluids due to the Marangoni effects can be effective in draining of the unswept regions. The dimensional analysis for possible mechanisms showed that the viscous, gravity and diffusion forces were negligible and the other mechanisms such as capillary and Marangoni effects should be considered in the investigated experiments. The value of the new defined Marangoni/capillary dimensionless number for the Na_2CO_3 solution was orders of magnitude larger than the $MgSO_4$ flooding scenario which explains the differences between the two cases and also between different micromodel regions. In conclusion, the Marangoni convection is activated by creating an ultra-low IFT condition in multiphase flow problems that can be profoundly effective in increasing the phase mixing and microscopic efficiency.

Keywords Marangoni effects · Chemical flooding · Surface tension · Alkaline

1 Introduction

Chemical flooding for the purpose of enhanced oil recovery (EOR) methods is gaining increased attention in recent years. As a chemical EOR method, alkaline flooding where different chemical species such as sodium hydroxide (NaOH) and sodium carbonate (Na_2CO_3) are dissolved in aqueous solution are known for their potential for improving oil recovery factor (Liu et al. 2008). In this method, the alkaline solution reacts with polar components of the oil (carboxylate branches and branches with oxygen and sulphur atoms) or polar sides of the rock leading to changes in the solid/fluid or fluid/fluid interfacial properties which, in turn, reduces the volume of trapped oil in the formation. Similar to the surfactant flooding method, the main mechanisms enrolling in alkaline flooding process are interfacial tension (IFT) reduction, wettability alteration, and emulsification (Sheng 2010). In oils with the higher amounts of organic polar components, such as heavy and asphaltic oils, the alkalines may work more efficient than surfactants (Mahdavi and Zebarjad 2018). The stated mechanisms usually change the contribution of effective forces which would then lead to a higher fractional flow of oleic phase with respect to the aqueous phase and lower trapping capillary forces (Mohammadi et al. 2009). The main advantage of this method over micellar flooding is its effectiveness and lower costs (Olajire 2014).

It is generally believed that the microscale and macroscale multiphase flow in porous media is greatly under the control of the main effective forces including viscous, capillary and gravity forces (Blunt 2017). The relative contribution

Edited by Yan-Hua Sun

Electronic supplementary material The online version of this article (https://doi.org/10.1007/s12182-020-00451-z) contains supplementary material, which is available to authorized users.

✉ Masoud Riazi
mriazi@shirazu.ac.ir

[1] School of Chemical and Petroleum Engineering, Shiraz University, Molasadra Avenue, 71946-84636 ShirazFars, Iran

of each mechanism is highly case-dependent (Herring et al. 2015) that was investigated by many researcher (Abbasi et al. 2017; Debbabi et al. 2017a, b). These mechanisms are also dependent upon the inherent architecture of the porous media. The order of magnitude of each mechanism is also imperative for the correct interpretation of the flow phenomena in porous media. In addition to the previously mentioned forces, recent studies revealed that the fluid flow in porous media also may be influenced by the Marangoni convection that is defined as the mass transfer along with an interface between the two phases because of a gradient of the surface tension (Alizadeh et al. 2014; Iervolino et al. 2019; Masoudi et al. 2019; Schmitt and Stark 2016). This mass transfer may lead to fluid flow and transport of fluids in the bulk (Baroud 2013). The Marangoni effects are mainly found in temperature gradient (thermal) and concentration gradient (solutal) forms at the interface of fluids (Velarde and Zeytounian 2002). The maintained stress generates a convective flux along with the interface of fluids (Park et al. 2020). Kim et al. (2017) analysed the spreading of two miscible phases due to the Marangoni convection and showed that the spreading velocity of the phases at their interface is a function of fluid properties such as viscosity, density, and IFT (Kim et al. 2017). Marangoni effects usually are characterized using a dimensionless number known as the Marangoni number that is defined as the ratio of surface tension force to molecular diffusive force (Yao et al. 1996):

$$Ma = \frac{(\mathrm{d}\sigma/\mathrm{d}C) \times \Delta C \times L_{\mathrm{m}}}{\mu \times D_{\mathrm{f}}} \quad (1)$$

where $\mathrm{d}\sigma/\mathrm{d}C$ is the change of interfacial tension with solvent concentration, ΔC is the gradient of concentration, L_{m} is the Marangoni characteristic length that sometimes is considered as the height of the domain, μ is the dynamic viscosity, and D_{f} is the diffusion coefficient. The Marangoni movement for the first time was reported by Clowes (1916) by observing a profound Brownian movement during emulsion tests. Castor and Somerton (1977) investigated the interfacial instabilities in flow in porous media in both gas/liquid and liquid/liquid interfaces and found that these processes can be promoted by several mechanisms such as the displacement of non-wetting phase by wetting phase, differences between viscosities of different phases, and also surface tension gradients in fluid interfaces that is appeared by appearance of surface-active materials.

Stebe and Barthès-Biesel (1995) investigated the impact of surfactant made Marangoni effects on a gas bubble in a capillary tube. They found that larger Marangoni numbers can simply influence the flow velocity which would, in turn, increase the drag forces at the interface. Lyford et al. (1998a) investigated alcohol injection and experienced increased oil recovery. They concluded that Marangoni-induced oscillation of the trapped organic phase was the possible reason behind the observed enhanced recovery. D'Aubeterre et al. (2005) studied the Marangoni effect induced by heat or mass transfer and clarified the Marangoni mass transfer in both cases. They found that with increasing pressure, the mass transfer due to the Marangoni effect increases. Also, they found that in lower carbon numbers the Marangoni force is more powerful due to increasing the perturbation sensibility and adsorption instability of oil/water interface at lower carbon numbers. Pratt (1991) suggested that the Marangoni effect could be utilized as an EOR mechanism when water injection is followed by solute injection. They stated that this mechanism would get more intense in water alternating gas (WAG) injection processes.

Khosravi et al. (2015) evaluated the impacts of Marangoni convection on oil recovery in a near-miscible CO_2 injection process. They introduced an interfacial tension gradient in the investigated system and found that the maximum influence of Marangoni flow during CO_2 flooding processes was visible at near-critical (pressure/temperature) conditions. Under such circumstances, the oil recovery was improved by about 35% due to Marangoni effects. Yunyun et al. (2016), using a micromodel study, investigated the positive impact of Marangoni force in decreasing residual oil saturation and improving the oil recovery in a chemical flooding process. By examining different alkaline solutions including Na_2CO_3, their experiments confirmed lower interfacial tension due to the reaction between basic solutions (Na_2CO_3) and an acidic component of crude oil that caused interfacial tension gradient and finally led to Marangoni convection. Furthermore, Troian et al. (1990) showed that the presence of Marangoni effects due to surfactant concentration gradient may lead to fingering instabilities. They also found that the surfactant mass transfer diffusion is too slow to affect the flow instabilities. Zhang et al. (2017) by utilizing a microscope and nuclear magnetic resistance (NMR) tool investigated the process of nanoemulsification in core-flooding and sand-pack flooding operations and found that the Marangoni effect can be considered as an effective mechanism in heavy oil EOR processes. This would consequently affect the emulsification process in the case of nanoemulsion flooding. Masoudi et al. (2019) in a gas flooding micromodel study showed that the thermal-induced Marangoni effect may help the injection stream to enter the unswept oil-saturated zone (e.g. dead-end pores and matrix/fracture systems) and increase the oil production. They concluded that the main reason behind this enhancement was the ability of the Marangoni effect in improving the mixing of phases by applying swirling flow velocities. Park et al. (2020) investigated the effects of solutal Marangoni effect on the mixing efficiency of sessile droplets and saw that the mixing of components significantly reduced if the Marangoni

force were applied. Abolhosseini et al. (2018) investigated the thermal Marangoni convection in a capillary dominated system and found that the Marangoni convection can overcome the capillary effects and cause the oil to flow in porous media.

In spite of previous studies to discern the impact of Marangoni force on multiphase fluid flow in porous media, there are still many unanswered questions on the topic of ultra-low IFT alkaline flooding. The main complexity for the characterization of Marangoni force in multiphase flow processes is the interference of it with other mechanisms like viscous or capillary forces. This complexity is boosted in EOR chemical flooding practices where several multiphase and interfacial processes occurred at the same time. In this work, using a transparent micromodel approach, the aim was to visually observe the Marangoni effects in alkaline flooding processes by innovatively controlling of other effective mechanisms. The potential impacts of Marangoni force in multiphase flow in the micromodel porous media and its potential roles in improving oil recovery is also studied. The impact of other forces in competition with Marangoni force is also discussed. In what follows, firstly, the materials and experimental procedures are introduced. Then, the experimental and theoretical results are discussed for both static and dynamic tests, separately.

2 Research methodology

Provided the presence of different dominant forces and mechanisms, then an accurate characterization of the contribution of each individual mechanism in chemical flooding would be highly complicated. Therefore, in this study, several experimental and numerical methods are sought to improve the quality and generality of the obtained conclusions.

Table 1 Properties and SARA fractions of the crude oil

Density, g/cm^3	Viscosity, cP	SARA analysis, wt%			
		Saturations	Aromatics	Resins	Asphaltenes
0.934	145	59.6	26.3	8.8	5.3

2.1 Experimental study

2.1.1 Crude oil and brine properties

Crude oil was obtained from one of the Iranian oil fields with a density and viscosity of 0.934 g/cm^3 and 145 cP at ambient conditions, respectively. Furthermore, the viscosities of all aqueous solutions were 1 cP at ambient conditions. Table 1 shows the SARA fractions (saturates, aromatics, resins, and asphaltenes) of the investigated crude oil.

Sodium carbonate (Na_2CO_3) and heptahydrate magnesium sulphate ($MgSO_4{\cdot}7H_2O$) were used for preparing brines with the required properties. These salts had different acidities and their purity was over 99% (Merck), see Table 2. With the aim of having a suitable IFT reduction, the high concentration of 50,000 ppm was selected, although the results can be achieved in the lower concentrations. Also, the IFT gradient, $\Delta\sigma$, expected in these processes are calculated as

$$\Delta\sigma = \sigma_{ao} - \sigma_{wo} \tag{2}$$

where σ_{ao} and σ_{wo} are the interfacial tensions between aqueous and oleic phases at the maximum (50,000 ppm) and minimum (0 ppm, pure water) concentrations of alkaline, respectively. Thus, the calculated IFT gradient is the difference occurred between two phases at its extreme conditions.

For the flooding tests, a semi-uniformly heterogeneous pattern was used in the micromodel. The geometrical characteristics of the micromodel are provided in Table 3. A geometrical schematic of the micromodel is also depicted in Fig. 1. It shows that the model vertically consists of three different porosity/permeability regions to gain some insights about the impacts of heterogeneities of the porous domain on the extent of Marangoni stresses.

2.1.2 IFT and contact angle tests

The IFT was measured by the pendant drop method using a DST-100 apparatus. The measurement was carried out with

Table 2 Properties of the aqueous phases

Fluid	Salt concentration, ppm	Density, g/cm^3	pH	IFT σ, mN/m	IFT gradient $\Delta\sigma$, mN/m	Viscosity, cP
Distilled water	0	0.997	7.0	30.21	0.0	1.00
Sodium carbonate	50,000	1.036	11.5	< 0.10	> 30.11	1.04
Magnesium sulphate	50,000	1.048	6.0	27.46	2.75	1.06

Table 3 Geometrical properties of the investigated micromodel

Micromodel type	Length, cm	Width, cm	Pore volume, m^3	Pore diameter, μm		
				Low permeability region	Intermediate permeability region	High permeability region
Semi-uniform pattern	6	6	0.6	200	250	350

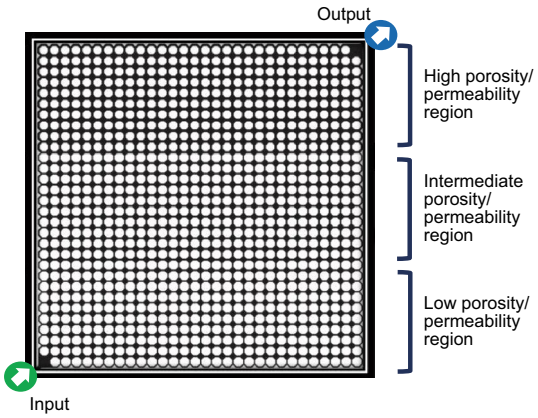

Fig. 1 Geometry of the micromodel

the method presented by Alnoush et al. (2019). The measured IFT values are listed in Table 2.

From Table 2, it can be seen that adding Na_2CO_3 alkaline reduced the interfacial tension between the oil and aqueous phases considerably and generated an ultra-low IFT condition. The tests were carried out at the ambient conditions (298.15 K, 1 bar), like performed on the micromodel tests.

The contact angles between fluids and glass were also measured using the DST-100 apparatus and the method documented by Alnoush et al. (2019) at ambient conditions. The used glass was let to be aged for one day (similar to the micromodel aging time) and then the contact angle between different couples of oil and brines including oil/Na_2CO_3, oil/$MgSO_4$, and oil/deionized water (DW) were measured. The goal of the aging process was initialization of the wettability of the glass for the used system of fluids.

2.1.3 Experimental procedure

Firstly, the Marangoni effect was investigated at static conditions. To do so, two containers were filled with Na_2CO_3 and $MgSO_4$ brines, separately. Then a droplet of crude oil was gently added using a syringe to each of the containers (the tests were established at 298 K). The interactions between the brine and crude oil were then recorded before analysing the images by the ImageJ software. The spherical assumption for droplets was set to be between 90 to 100 percent in the software for further precise analysis.

The above measurements were followed by micromodel tests. Figure 2 shows a schematic of the experimental set-up used in this study. The precise injection of fluids into the micromodel was accomplished using an LA-30 syringe pump which was capable of injecting fluids with the rates up to 125 mL/h. Using a HLOT microscopic camera, fluid flow was carefully monitored in the micromodel. A Tecl LED backlight panel was also used to enhance the quality of images and videos.

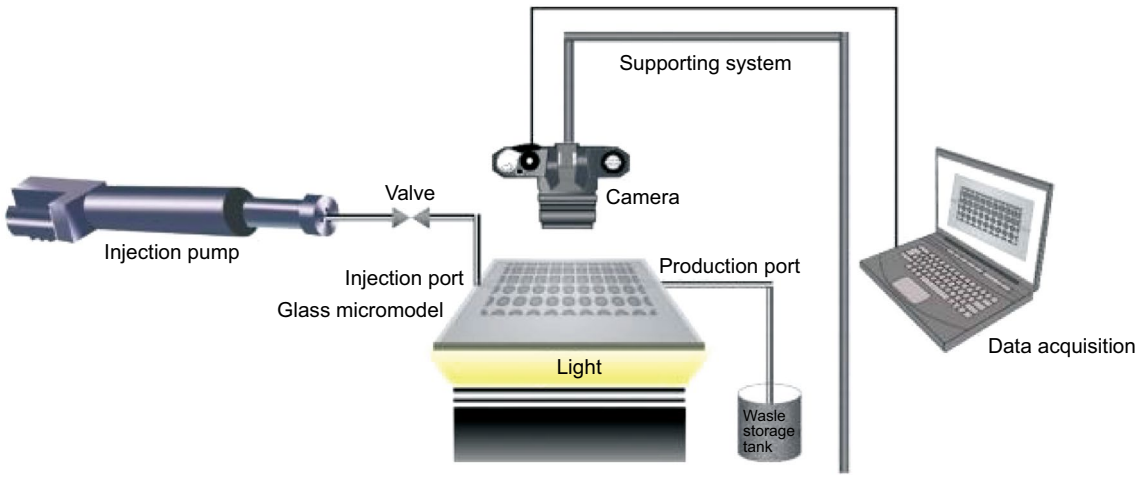

Fig. 2 Schematic of the experimental micromodel set-up (Kazemzadeh et al. 2015)

The investigated fluids in the experiments were crude oil, DW, 50,000 ppm of Na_2CO_3 brine, and 50,000 ppm of $MgSO_4$ brine (Table 2). These concentrations were just enough to discern the potential effects of the used salts on the multiphase flow in the micromodel. The micromodel was aligned horizontally and the effects of gravity were removed. Then, the initialization of the micromodel was performed by injection of DW followed by the crude oil to the micromodel until the stable initial condition was reached (no water was produced and the micromodel was fully saturated with oil). All tests were conducted at ambient conditions. Also, to eliminate any thermal Marangoni effects, the temperature of all the fluids and micromodels was initialized at 298 K. Moreover, the chemical flooding tests were carried out by injection of the displacing fluids (i.e. Na_2CO_3, and $MgSO_4$ brines) with the rate of 80 mL/h. The injection stopped after 60 s and the fluid interactions and fluid distribution change were monitored over time. The details of these tests are provided in Table 4. It should be indicated that to ensure the reliability and reproducibility of the results, the tests were repeated for 3 times.

2.2 Image analysis

To analyse the number of emulsions in the static tests the ImageJ software was used. After importing the obtained picture to ImageJ, the blurriness of pictures, friskiness and other factors which decreased the quality of pictures were omitted automatically to some extent. Hence, the quality of the images was improved significantly. Finally, the pictures were transformed to binary pictures and then analysed to find the number of emulsions.

For quantitative analysis of the micromodel results and tracking the injection front, an image processing algorithm (Dong and Selvadurai 2006; Roman et al. 2016; Zuo et al. 2013) was used using MATLAB Image Processing Toolbox (Davis 2004). The used colour model was a Red–Green–Blue (RGB) and the analysis was conducted using histogram curves for distribution of pixel colours in the micromodel. After calibrating the colour range of each phase by determining phase boundaries (pore, brine, and oil), the number of pixels related to each phase was determined and the saturation of each phase in the micromodel was calculated. The maximum error in the calculated results was around than 2% of the oil saturation with respect to those of the calibration results.

Table 4 Summary of the micromodel alkaline flooding tests

#	Test name	Flooding rate, mL/h	Flooding time, s	Injection volume, PV
A	$MgSO_4$ flooding	80	60	0.62
B	Na_2CO_3 flooding	80	60	0.62

3 Results and discussion

3.1 Static experimental tests

As stated earlier, the fluid flow in porous media may be under the influence of several mechanisms such as viscous flow, gravity flow, capillary imbibition or drainage, and wettability alteration. Sometimes, the boundaries between these mechanisms are not readily distinguishable. In this study, firstly, to simplify the investigation process, a static test was conducted, in which a droplet of oil was slowly placed at the interface of a liquid bath full of $MgSO_4$, and Na_2CO_3 brines with the concentrations of 50,000 ppm, in two separate experiments. The exerted condition was such that no considerable viscous forces were applied to the investigated system. Under such circumstances, the impact of gravity, viscous and capillary forces can reliably be ignored. Also, molecular diffusion can be easily ignored because of its time-consuming process (Sakai et al. 2002).

Figure 3 (see the electronic supplementary videos 1 and 2) shows the behaviour of two defined systems versus time after placing the oil droplet on the interface of the aqueous phase. As the figure shows, the oil droplet approximately stayed uniform and kept its initial shape versus time in the $MgSO_4$ brine (Fig. 3a–c), while in the Na_2CO_3 solution, the oil droplet firstly spread on the surface of the alkali aqueous phase and then a long twirling flow was observed (Fig. 3d–f). The differences between the behaviour of the oil droplets in two systems can be interpreted by considering interfacial properties of both systems. The most important difference between the two systems is the IFT between the oil and aqueous phases. Figure 4 shows the drop shapes of the oil with different aqueous solutions in the pendant drop interfacial test. As it can be seen, the drop shape for oil/distilled water and oil/$MgSO_4$ solution are almost similar, while the droplet of the oil/Na_2CO_3 solution is considerably smaller such that the IFT cannot be measured by the present DST-100 apparatus.

Table 2 shows the IFT values of the used aqueous phases. It can be concluded that by adding Na_2CO_3 solution, an IFT gradient around 30.11 mN/m may be applied to the interface of the fluids. By spreading of the oil on the interface of the brine, a regional IFT gradient at the fluid/fluid interfaces appears. This IFT gradient can activate the Marangoni force around the oil/brine/air interface. The Marangoni convection would then lead to a fast, circular, and erratic flow. The results of these simple tests show that Marangoni effect possibility presents when different fluids including chemicals, water, and oil

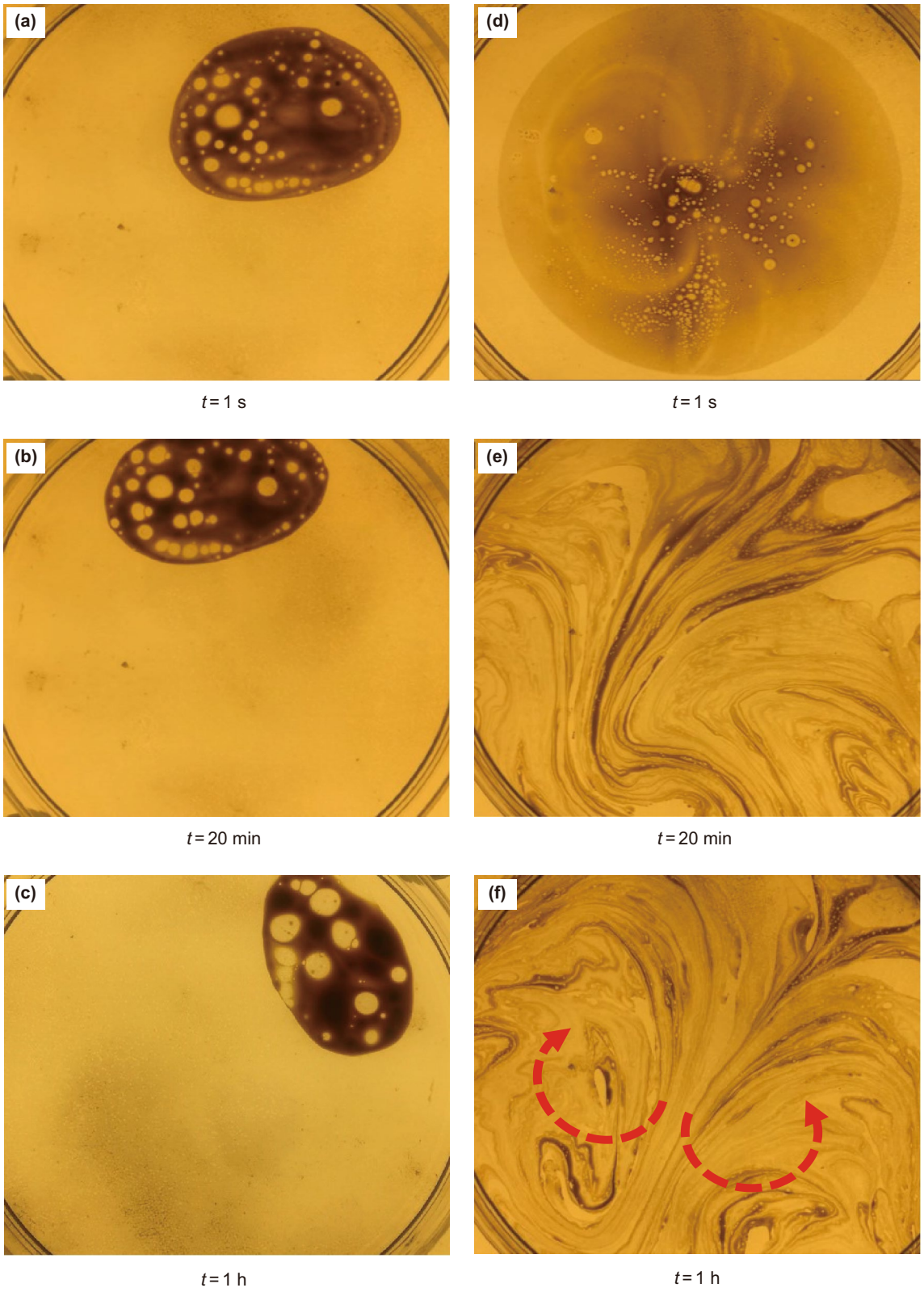

Fig. 3 Flow trends in two different fluid mixtures of **a–c** 50,000 ppm $MgSO_4$ brine (electronic supplementary video 1), and **d–f** 50,000 ppm Na_2CO_3 brine (electronic supplementary video 2)

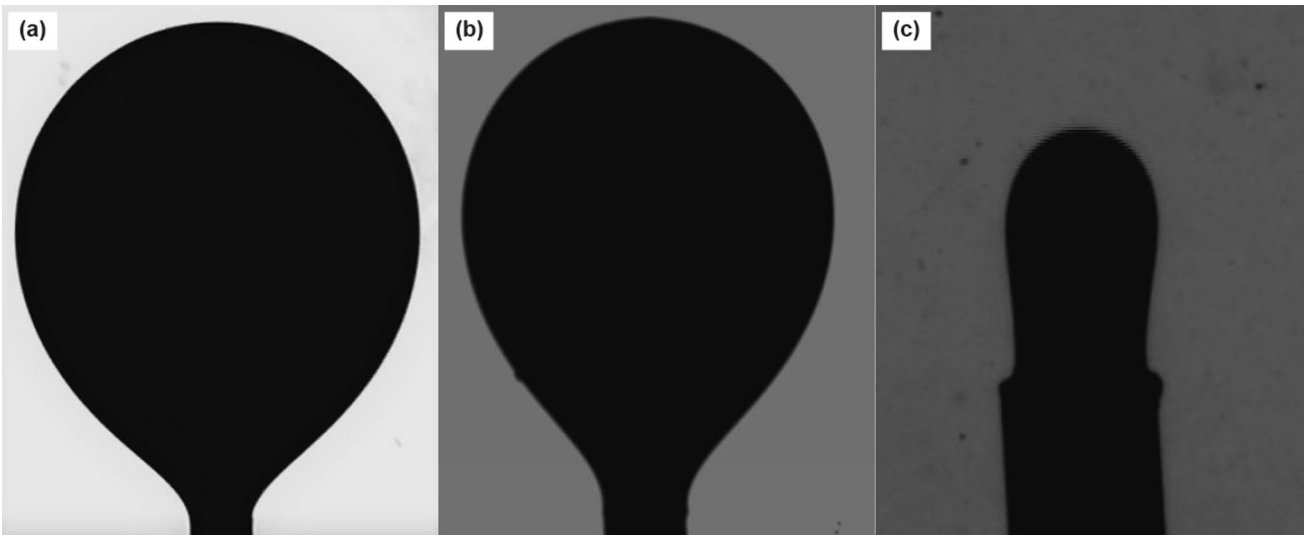

Fig. 4 Pendant drop images for measurement of IFT between the oil and aqueous solutions ($T = 298$ K). **a** Oil and distilled water. **b** Oil and $MgSO_4$ solution at 50,000 ppm. **c** Oil and Na_2CO_3 solution at 50,000 ppm

are being in contact with each other, for instance, a chemical enhanced oil recovery (EOR) process.

A closer look at the results of static tests reveals that an intense movement was expected to occur as the oil droplet touches the alkali solution. This is because of interactions between acidic components of oil (i.e. asphaltene components) and basic solution which produced in situ surfactants (Gong et al. 2017). Figure 5 demonstrates the spreading of the oil droplet in the Na_2CO_3 solution in less than one second. The main mechanism behind this fast spreading is the Marangoni convection due to the generated gradients in interfacial tension of fluids. A likely schematic related to this gradient is shown in Fig. 6a. The IFT between the oil/water interfaces is much lower than that between the air/water interface that leads to the flow from the point with lower IFT to the point with higher IFT. This IFT gradient results in a high Marangoni number, thus a fast fluid movement would be expected to occur. The stated IFT gradient would be reduced during the spreading process that leads to reducing the spreading velocity. Table 5 shows the calculated Marangoni number for both cases. As it shows, the magnitude of Marangoni number is considerable in both cases, although it is about one order of magnitude larger in the case of oil spreading in the Na_2CO_3 solution. The spreading phenomenon due to the Marangoni-driven convection is usually characterized by the spreading coefficient that is defined as (Wang et al. 2018):

$$S = \sigma_{aw} - (\sigma_{ow} + \sigma_{oa}) \tag{3}$$

where the subscripts of o, w, and a are the representation of oil, water, and air phases, respectively. If $S > 0$, the spreading occurs and continues until the S becomes zero (Kim et al. 2017). Table 6 provides the spreading coefficients calculated for both alkalines and shows that the value of spreading coefficient is positive for both cases, although for Na_2CO_3 solution it is greater. This is a good indication of the power of the Marangoni effect in both cases that well matches with the experiments.

On the other hand, it can be observed in Fig. 5 that the number of emulsions increases continuously during the spreading of the oil droplet (electronic supplementary videos 3 and 4). The number of generated emulsions (in the Na_2CO_3 solution) is larger than the number of emulsions in the $MgSO_4$ solution (Fig. 3a and d). This can be due to the lower interfacial tensions and the interface turbulences occurred in the course of Marangoni convection. A similar observation was also found by Zhang et al. (2017) in a polymer flooding process. Figure 7 shows the number of generated water/oil (W/O) emulsions in the Na_2CO_3 solution during the spreading of an oil droplet on alkali surface versus area of emulsions which analysed by the ImageJ software. The figure shows the number of the total produced W/O emulsions after 0.4 s is 66 (Fig. 5c), while this frequency reached to 158 only after 1 s in Fig. 7b (which corresponds to Fig. 5f). It can also be observed that in addition to the increased frequency (both in total and the same area), the area of droplets enlarged sharply. According to Fig. 6, it can be explained that the Marangoni convection would promote the dispersion of oil droplet on the alkali surface. Hence, the produced in situ surfactant moves to the interface which would, in turn, cause low interfacial tension instantly and improved emulsification process. Thus, the significance of the Marangoni spreading force on the flow behaviour of phases with respect to each other is shown with the static

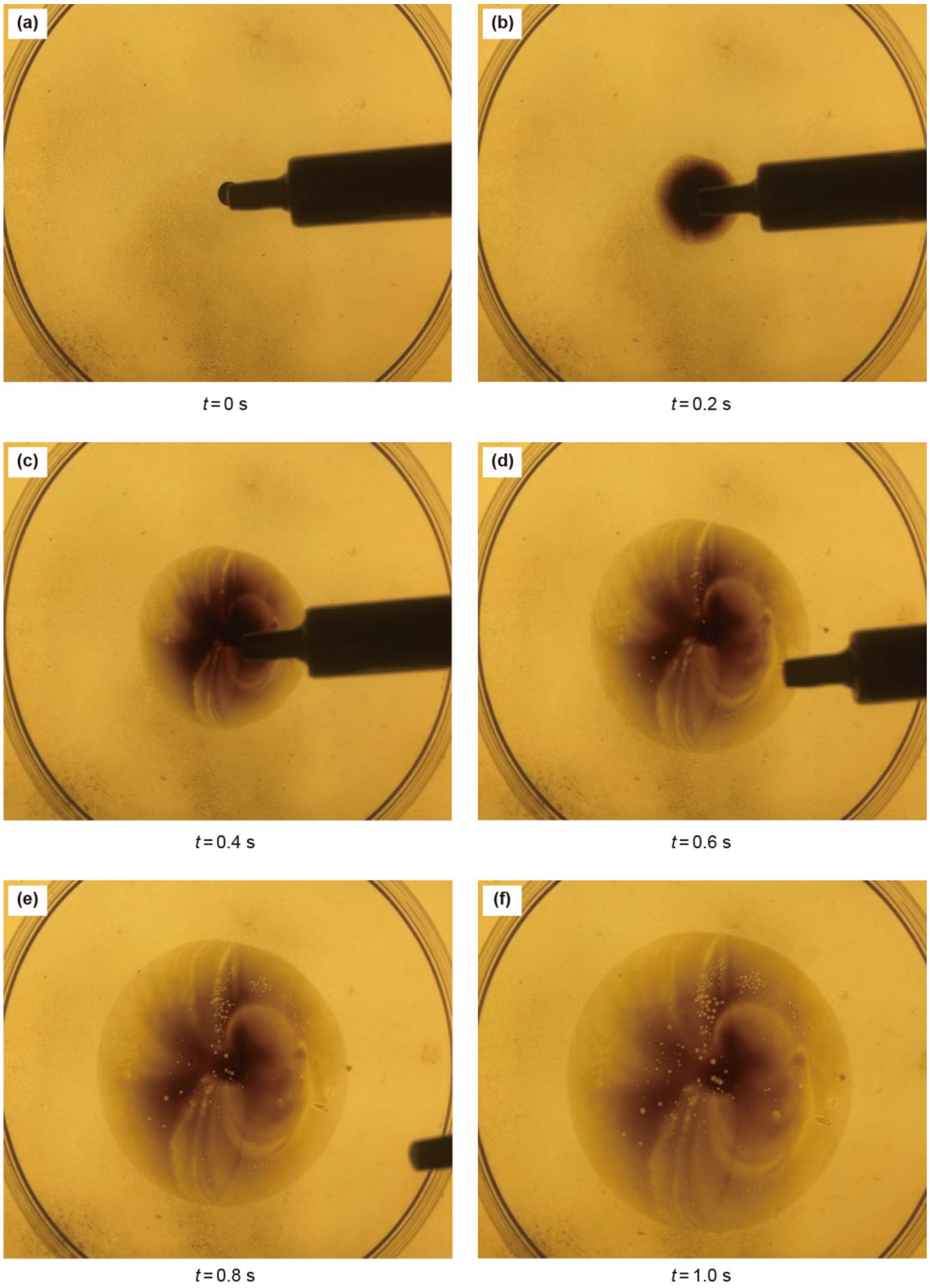

Fig. 5 Spreading of the oil droplet in the Na_2CO_3 solution. For more details, see the electronic supplementary videos 3 and 4

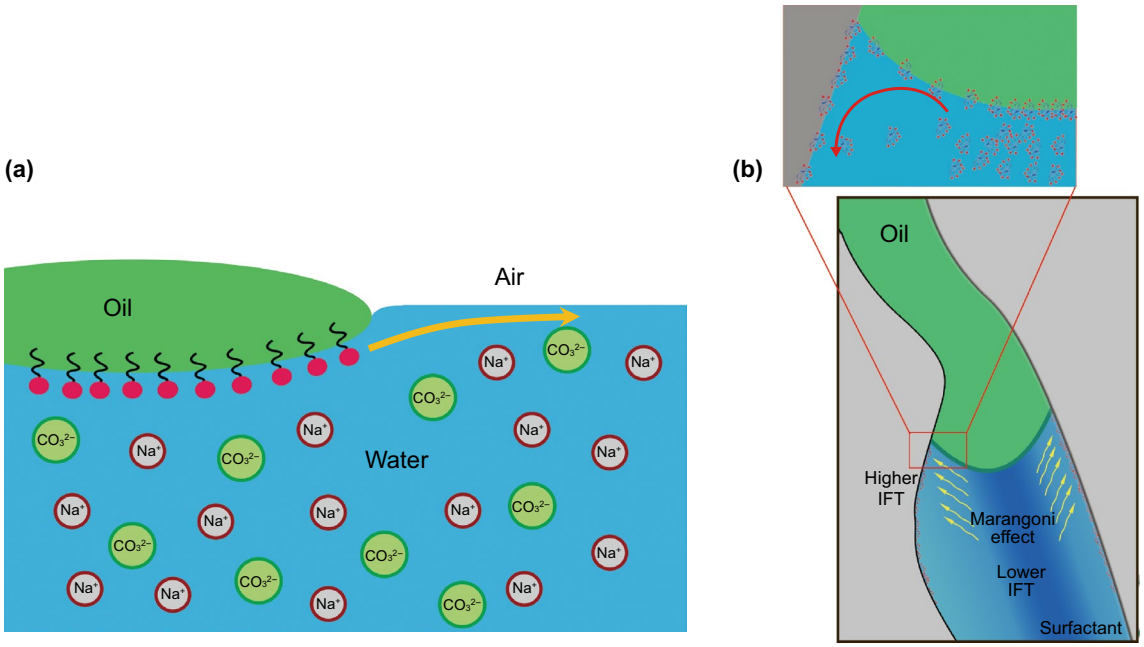

Fig. 6 Mechanism of solutal Marangoni convection in different flow geometries (the arrows show the flow direction). **a** At the interface of aqueous brine. **b** In a pore body

Table 5 The Marangoni dimensionless number (*Ma*) for different alkaline flooding scenarios

Used chemical	Diffusion coefficient, m^2/s	Characteristic length, m	Water viscosity, cP	IFT gradient, mN/m	Marangoni number *Ma*
Na_2CO_3	1.39×10^{-9}	2×10^{-4}	1.04	> 32.2	$>4.33\times10^{6}$
$MgSO_4$	0.67×10^{-9}	2×10^{-4}	1.06	2.21	6.60×10^{5}

Notes: The height of the micromodel was used as the Marangoni characteristic length (L_m). The diffusion coefficients used were from Gong (2012)

Table 6 Spreading coefficient for different alkaline flooding scenarios

Used chemical	Oil/air IFT, mN/m	Oil/water IFT, mN/m	Water/air IFT, mN/m	Spreading coefficient, mN/m
Na_2CO_3	23.51	< 0.10	54.75	> 31.14
$MgSO_4$	23.51	27.46	54.24	3.27

tests. In the following section, the effect of Marangoni force in micromodel tests is discussed.

3.2 Dynamic experimental tests

The alkaline flooding in porous media is used to change the fluid/fluid interfacial properties and the rock wetting properties. These mechanisms were investigated thoroughly by other researchers (Sheng 2017). The Marangoni convection can also occur due to various reasons: mixing of connate water with the injection fluid leading to dilution of the injected water. The adsorption of the injected brine on the solid surface could also lead to local concentration gradients in the bulk of the fluid. All of these effects could lead to some gradients in both the concentration and other properties like interfacial tensions that would cause the Marangoni convection (Lyford et al. 1998b). Thus, the contribution of Marangoni effects during chemical flooding in porous media needs to be studied. In this section, a micromodel was used to inject two different alkaline solutions (i.e. Na_2CO_3 and $MgSO_4$). As it was discussed in the preceding sections, at first, the alkaline solution was injected for one minute, then the distribution of fluids was traced when the injection was stopped. Figure 8a, c shows the initial times after stopping the injection of $MgSO_4$ and Na_2CO_3 solutions, respectively. As can be seen from Fig. 8b, in $MgSO_4$ solution flooding, the distribution of fluids was almost unchanged after 24 h. While, after stopping the injection of Na_2CO_3 solution, Fig. 8d, a spontaneous movement of fluids in the porous medium was observed (also see electronic supplementary video 5). A specific part of the micromodel for the above tests (the upper left of the micromodel) is shown in Fig. 9.

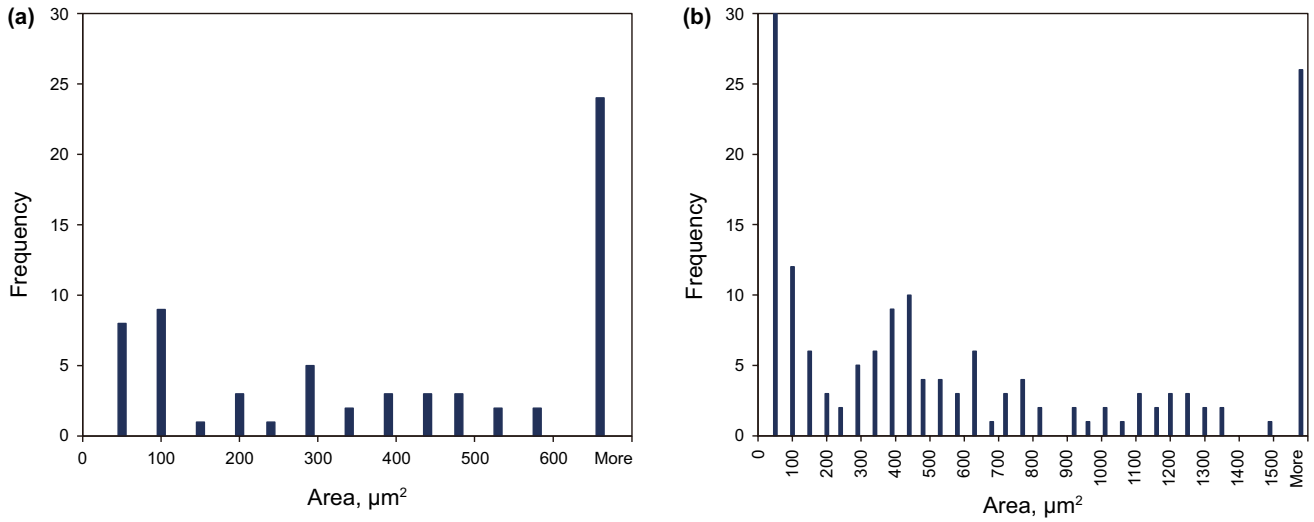

Fig. 7 Frequency of generated W/O emulsions versus the area of the emulsions during spreading of an oil droplet on the surface of Na_2CO_3: **a** after 0.4 s and **b** after 1 s

The distribution of fluids in the case of $MgSO_4$ flooding almost remained stationary, but this area was swept by the injected fluid in the case of Na_2CO_3 flooding. For better observation of the discussed phenomenon, it is recommended to watch the electronic supplementary video 5 that shows the disturbing flow of Na_2CO_3 solution within different regions of the micromodel after stopping the injection process. Most parts of the movement occurred in less than an hour period after stopping the injection. The interpretation of the reasons behind the observed phenomenon requires considering all the possible mechanisms that can be engaged in this process. These mechanisms can range from molecular diffusion to viscous and gravity forces that are separately discussed.

4 Dominant mechanisms

The flow in porous media can be controlled by different mechanisms that sometimes can work in opposite directions. The interpretation of the movements occurred in the experimental part of this study requires scrutiny of possible mechanisms to ensure that no potential mechanism is neglected. The viscous force, gravity force, capillary force, wettability alteration, and mass diffusion are among the most influential mechanisms. In micromodel experiments conducted in this work, after the termination of injection, the viscous force was negligible because of the absence of any pressure gradient within the inlet/outlet points. In addition, due to the small height of the micromodel, the gravity force can easily be ignored. The other potential mechanisms are scrutinized and discussed below.

4.1 Mass diffusion

Due to the presence of concentration gradients, molecular diffusion should be expected as the dominant mechanism in chemical flooding processes. The molecular diffusion is usually considered as a slow process in macroscopic scales because of the small magnitude of the diffusion coefficients (Masoudi et al. 2019; Nagumo et al. 2008; Ramírez-Muñoz et al. 2012). According to the first Fick's first law, the time required for diffusion of species with diffusion coefficient D_f into the distance d can be calculated by d^2/D_f (Paul et al. 2014). Using this relationship, the time required for diffusion of the particles within a 2.0 cm distance (about 1/5 of the length of the micromodel) is calculated. The diffusion coefficients used in this table are reported by Gong (2012). As Table 7 shows, the transport of the related species takes long about 79.94 h for Na_2CO_3 and 165.84 h for $MgSO_4$ that is considerably more than the time scale of the spontaneous movement observed in the micromodel experiment that was less than 1 h. The estimated mean velocity of the species due to molecular diffusion (i.e. 0.00020 cm/min for $MgSO_4$ and 0.00042 cm/min for Na_2CO_3) is considerably lower than the observed mean velocities in the micromodel (around 0.022 cm/min for Na_2CO_3 solution). From this large difference, it can be inferred that the molecular diffusion cannot be the reason behind the observed movement of fluids in the micromodel hence other mechanisms should be scrutinized.

4.2 Capillary pressure

Capillary pressure is defined as the pressure difference between two immiscible fluids occupied the same pores. This force controls the distribution of phases in the porous

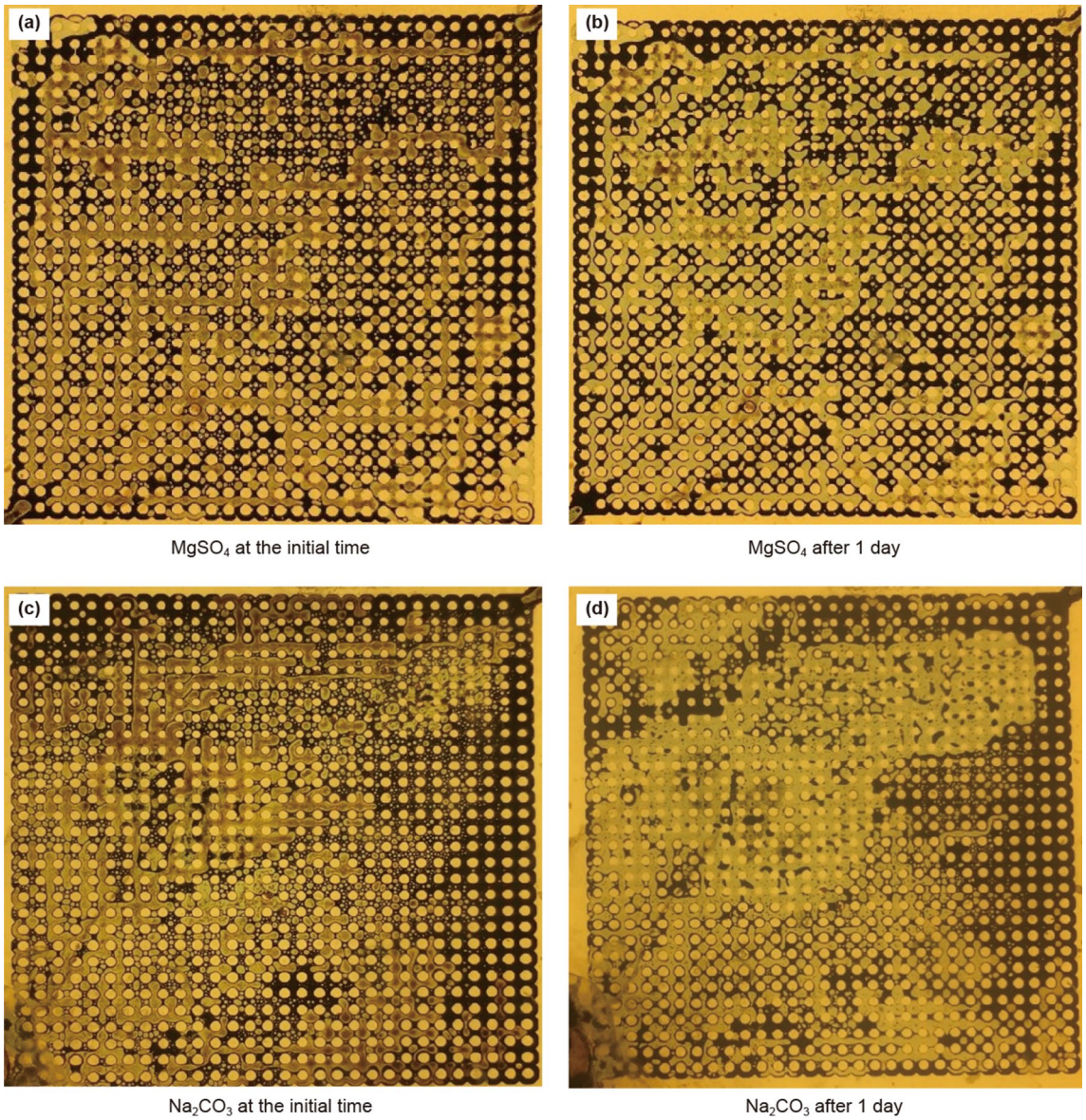

Fig. 8 Fluid flow in the micromodel after stopping the injection of the 50,000 ppm $MgSO_4$ and Na_2CO_3 solutions. For more details, see the electronic supplementary video 5. **a** $MgSO_4$ at the initial time. **b** $MgSO_4$ after 1 day. **c** Na_2CO_3 at the initial time. **d** Na_2CO_3 after 1 day

media. This force is depended on the fluid/fluid (IFT) and fluid/solid (contact angle) interfacial properties and also the pore geometry (Dandekar 2013):

$$P_c = \frac{2\sigma \times \cos\theta}{r} \tag{4}$$

where σ is the interfacial tension, θ is the contact angle, and r is the pore radius. It is common to check the relative dominancy of forces in the absence of viscous effects using the dimensionless inverse bond number (Bo^{-1}) that is defined as the ratio of the capillary to gravity forces (Herring et al. 2015):

$$Bo^{-1} = \frac{\sigma}{\Delta\rho \times g \times d^2} \tag{5}$$

where $\Delta\rho$ is the density difference between the phases, g is the acceleration of gravity and d is the representative length scale. The relative value of viscous drag to surface tension forces is compared with the capillary number that is defined as below (Herring et al. 2015):

$$N_{ca} = \frac{\mu \times v}{\sigma} \tag{6}$$

where v is the characteristic velocity of the fluids in the system. In the absence of the injection in the micromodel tests,

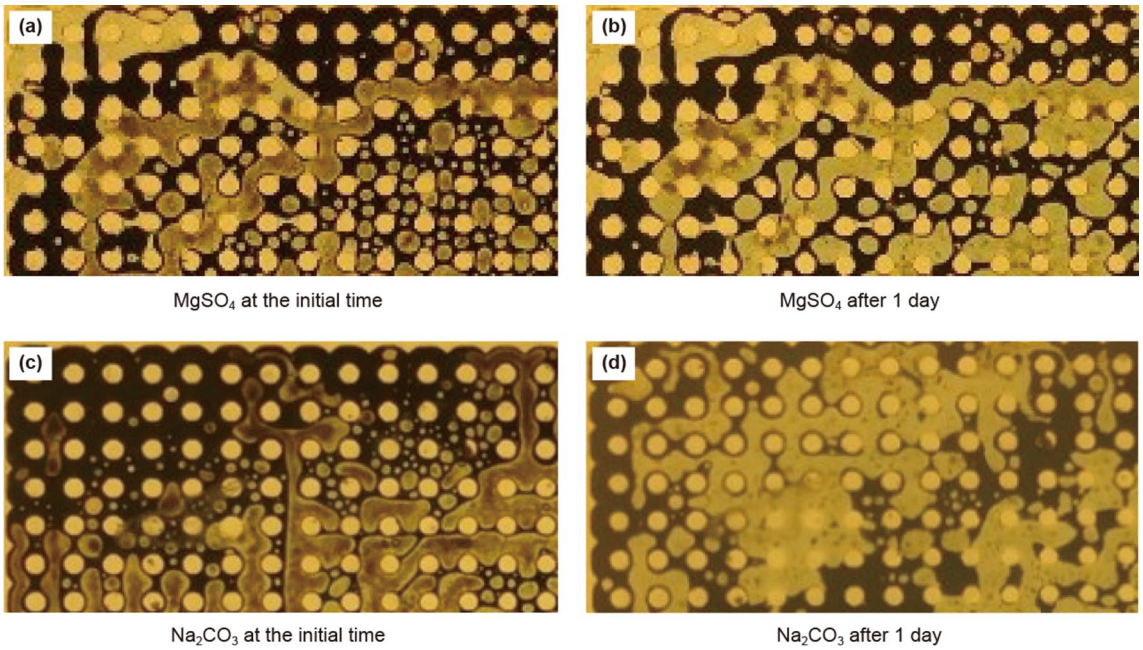

Fig. 9 Distribution of the fluids in a specific part of the micromodel (upper left) after stopping the injection of the 50,000 ppm $MgSO_4$ and Na_2CO_3 solutions. For more details, see the electronic supplementary video 5. **a** $MgSO_4$ at the initial time. **b** $MgSO_4$ after 1 day. **c** Na_2CO_3 at the initial time. **d** Na_2CO_3 after 1 day

Table 7 Calculated diffusion time of alkaline through a given distance

Solution	Temperature, K	Diffusion coefficient, m^2/s	Diffusion distance, cm	Calculated diffusion time scale, h	Mean calculated diffusion velocity, cm/min	Mean observed velocity, cm/min
$MgSO_4$	298.0	0.67×10^{-9}	2.0	165.84	0.00020	0.00
Na_2CO_3	298.0	1.39×10^{-9}	2.0	79.94	0.00042	0.02

Notes: The mean diffusion velocity was calculated based on the diffusion coefficient and the mean observed velocity was calculated based on the velocity of movements of the front after stopping the injection of the related alkaline

the viscous velocity and consequently the value of the capillary number is zero.

The wettability of solid would potentially be a prevailing factor in the capillary behaviour of fluids in the porous media. It is shown that during alkaline flooding, the oil recovery can be improved due to alteration of solid/fluid wetting properties by adsorption of the in situ formed surfactants on the pore surface (Gong et al. 2016). The results of the contact angle tests are shown in Fig. 10 from which it can be seen that the wetting condition of the glass is water-wet ($\cos\theta > 0$) for the oil/DW and oil/$MgSO_4$ solutions, and is oil-wet ($\cos\theta < 0$) for oil/Na_2CO_3 solution. The oil drop in the Na_2CO_3 solution spread on the glass surface due to its low IFT (Gong et al. 2016). The measured contact angles can be a good indication of the wettability of the glass in the micromodel for both alkalines. Furthermore, as Fig. 11 shows for the Na_2CO_3 flooding scenario, the pore spaces of the micromodel was initially surrounded by the crude oil in all domains of the micromodel. This can be an indication for the initial wettability of the pore surfaces at early time after stopping the injection. Moreover, the figure shows that the affinity of pore walls with respect to oil maintained after 24 h while this period is enough for seeing any changes in wetting properties of the surface. Although the wettability of the micromodel cannot be a reason for the observed phenomenon by itself, the effects of wettability on the capillary behaviour of fluids cannot be ignored. The values of contact angle are shown in Table 8. It states that the capillary pressure would have a negative value for Na_2CO_3 flooding and have a positive value for $MgSO_4$ flooding. In the case of Na_2CO_3 flooding, since it can be assumed that the pore walls are oil-wet, the injected brine would serve as non-wetting phase ($\cos\theta < 0$) resulting in negative value

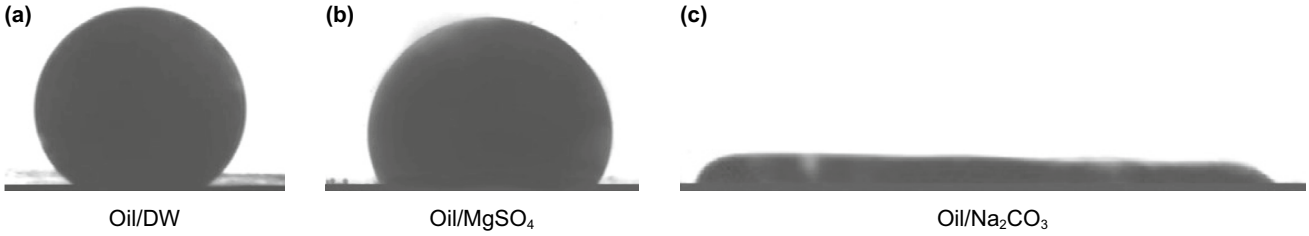

Fig. 10 Images for measurement of the contact angle between the oil and aqueous solutions. **a** Oil and deionized water. **b** Oil and $MgSO_4$ solution at 50,000 ppm. **c** Oil and Na_2CO_3 solution at 50,000 ppm

of capillary pressure. Thus, the capillary force acts as a resistance in letting the alkaline to enter the pores filled by oil.

Table 8 also shows the magnitude of capillary pressure for different scenarios in different micromodel zones. As the wettability of the solid, the P_c is negative for Na_2CO_3 flooding, because of ultra-low IFT, the P_c value is too low. Moreover, due to more pore throat radius, the absolute value of the capillary effect in the high permeability zone ($r = 200$ µm) is lower than its value in low permeability zone ($r = 100$ µm). Having considered this fact then it is expected that the sweep efficiency of oil in the high permeability zone would be higher. Overall, in the case of Na_2CO_3 flooding, the value of capillary pressure is negligible and since it has the negative value, it is a resistance force against the flooding fluid hence cannot be the main mechanism for the observed phenomenon. In the case of $MgSO_4$ flooding though, its value is positive but still, it does not seem its value is enough for the generation of a spontaneous imbibition flow within the micromodel. As a matter of fact, if the capillary pressure was effective, then the flow would have happened in the $MgSO_4$ case, not the Na_2CO_3 flooding. Also, the calculated values are less than the effective ranges observed in the previous studies (Abolhosseini et al. 2018; Schmid et al. 2012).

4.3 Gravity segregation

To analyse the effects of gravity force on the micromodel tests, the inverse bond number values for different scenarios were calculated, as shown in Table 8. The calculated inverse bond number also shows that the capillary pressure is dominant in comparison to gravity force (it should be considered that the value of the capillary force is negligible). The low height of the micromodel ($h = 0.2$ mm) does not allow any water/oil segregation to occur in the micromodel, so the magnitude of gravity can be excluded in the analysis.

4.4 Marangoni convection

As explained earlier, the conventional flow mechanisms like viscous, gravity and capillary forces cannot be the main reason behind the phenomenon observed in the micromodel experiments. The Marangoni force is another potential phenomenon that needs to be scrutinized. Various studies showed that the presence of a surface tension gradient can generate significant stress along with the interface of fluids that leads to a sharp velocity near the interface. Since the main role of surface-active materials is to manipulate the IFT between the fluids, the Marangoni force can be activated at interfaces where surfactants would not distribute uniformly. By comparing the results of pendant drop tests that are shown in Table 2 (Fig. 4), it can be observed that adding $MgSO_4$ did not change the IFT between oil and brine considerably (only about 7%) while adding Na_2CO_3 to the injecting water reduced the IFT as much as 99%. Such profound differences in IFT would indicate the impact of Marangoni force when the Na_2CO_3 solution is flooded in the micromodel (Yunyun et al. 2016).

The chemical properties of the injected fluids imply that due to the low interactions between the $MgSO_4$ solution and oil components, a quasi-stationary condition should be anticipated. In alkaline flooding (Na_2CO_3 solution), though, it can be inferred that the movement of fluids (as it was discussed in the preceding section) was due to the concentration gradient of alkali solution at the oil/water interface which caused interface instability. Due to asymmetric interactions of fluids, a variety of concentration gradients can appear that would cause different convection phenomena like capillary pressure and Marangoni convection (Fig. 8b). In the absence of any viscous or gravity forces, understanding the reasons behind the observed fluid movement in Fig. 8 requires attention to the possible interfacial tension gradients that may exist at the brine/oil interfaces during chemical flooding and also the capillary forces in the micromodel.

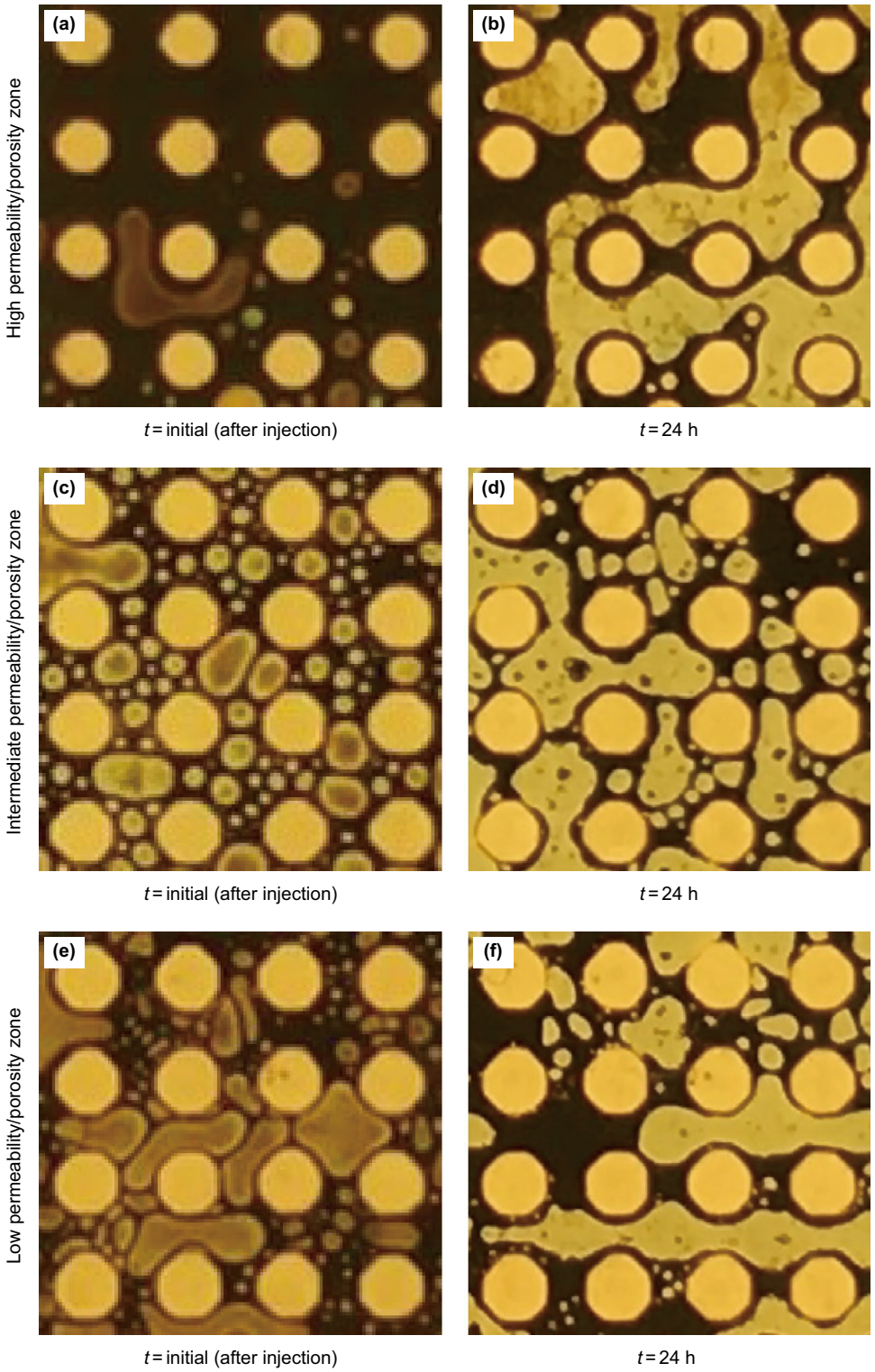

Fig. 11 Wetting behaviour of pore surfaces of the micromodel at different zones and times in the case of Na_2CO_3 flooding: The pores are wetted by the oleic phase; **a**, **b** high permeability/porosity zone, **c**, **d** intermediate permeability/porosity zone, and **e**, **f** low permeability/porosity zone

To investigate the influences of Marangoni-driven convection on unswept regions, the high and low permeability regions of the micromodel are compared in Fig. 12.

Figure 12a and f shows the different regions of the micromodel (high and low permeability/porosity zones, respectively) at initial times. As it can be seen from Fig. 12b, in the

Table 8 Capillary pressure in different regions of the micromodel with various injecting fluids

#	Injection brine	Micromodel region	Wetting phase	Pore radius, μm	IFT, mN/m	Contact angle, degree	Capillary pressure, Pa	Inverse bond number
1	Na_2CO_3	Low permeability	Oil	100	< 0.10	125	< –1.15	< 5.00
2		Intermediate permeability	Oil	150		125	< –0.76	< 3.33
3		High permeability	Oil	200		125	< –0.57	< 2.50
4	$MgSO_4$	Low permeability	Water	100	27.46	58	296.72	1399.13
5		Intermediate permeability	Water	150		58	197.84	932.76
6		High permeability	Water	200		58	148.38	699.57

Notes: The capillary number in all cases is negligible

high permeability/porosity region of the micromodel, after about 20 min, the alkaline solution moved to the upswept zone (left side) and in Fig. 12c the movement continued to the left and right sides simultaneously. Figure 12a, d and e also demonstrates that most of the fluid movements occurred in the first hours after stopping the injection (4 h) and the distribution of fluids remained almost constant after 1 day. This confirms that the production of surface-active agents decreases after a short period of time. Therefore, the IFT gradient would gradually be reduced until the Marangoni convection is stopped by disappearing any gradients in IFT. This process is similarly visible in the low permeability/porosity region of the micromodel that is shown in Fig. 12, where most of the fluid displacements occurred during the first hour of the test. In this region, the basic solution moved to the oil-saturated zone that was not swept by viscous forces, although this range of movement was less than the high permeability/porosity region. The results indicate that Marangoni convection forces can be effective in reducing residual oil saturation and increasing the sweep efficiencies. This would have implication in chemical flooding processes where the remained oil needs to be moved as much as possible and other mechanisms like wettability alteration and IFT reduction would not be enough to produce the entrapped oil.

Figure 12 also graphically illustrates that in the Na_2CO_3 solution flooding, the movement of fluids in high permeability/porosity zones is more than that in the low permeability/porosity zones. The attempted image analysis confirms this behaviour as shown in Fig. 13. In Fig. 13b, the trend of oil saturation for especial parts (sections I, II, and III of the micromodel in Fig. 13a) of the micromodel with different pore sizes is provided; where the oil saturation in the high permeability/porosity zone is reduced as well as the intermediate permeability/porosity zone. Nonetheless, in the low permeability/porosity zone, the oil saturation experienced a slow ascending trend. The reason behind this phenomenon can be attributed to the size of the interfacial area between oil and alkaline and the capillary behaviour of fluids. As the interface in the high permeability/porosity region is more than that in the low permeability/porosity region, then the reactions happen more intensely. Therefore, the produced surface-active materials decrease the interfacial tension and trigger stronger Marangoni effect due to the greater interfacial tension gradient. This behaviour lead to transferring of the remained oil from unswept regions to the flooded regions and improving the mixing of the phases. Also, the impacts of Marangoni convection in flooding of unswept regions of the porous media (regions III and IV) are comparable in Fig. 13c. In both regions, the oil saturation decreases. Reducing the oil saturation in the high permeability/porosity region is more than that in the low permeability/porosity one.

More discussions about the effects of pore geometry on the Marangoni flow is provided in the following.

Another reason for this observed behaviour would be due to capillary forces. The wetting behaviour of the pore surface (oil-wet) would implicate a negative value for the capillary force which is a resistive force in letting alkaline to enter the unswept zones. Since the absolute value of capillary pressure in high permeability zone is less than other zones (Table 8), less force is required to enter the brine to the oil-saturated pores in this zone. Overall, it can be summarized that the Marangoni and capillary forces are the flow controlling mechanisms in this process as such that higher Marangoni force along with the less capillary force leads to reduced oil saturation in higher permeability zones. It seems that the relative dominance of the Marangoni and capillary forces are the main factors contributing to the flow in porous media that was not considered in the Marangoni number. Hence, in this work, a new dimensionless number is proposed to compare the Marangoni and capillary forces:

$$\psi = \frac{Marangoni}{Capillary} = \frac{\partial\sigma \times r}{\sigma \times L_m} \tag{7}$$

where L_m is defined as the Marangoni characteristic length, and r is the pore throat radius. In this work, the micromodel height is assumed as L_m for the investigated alkalines

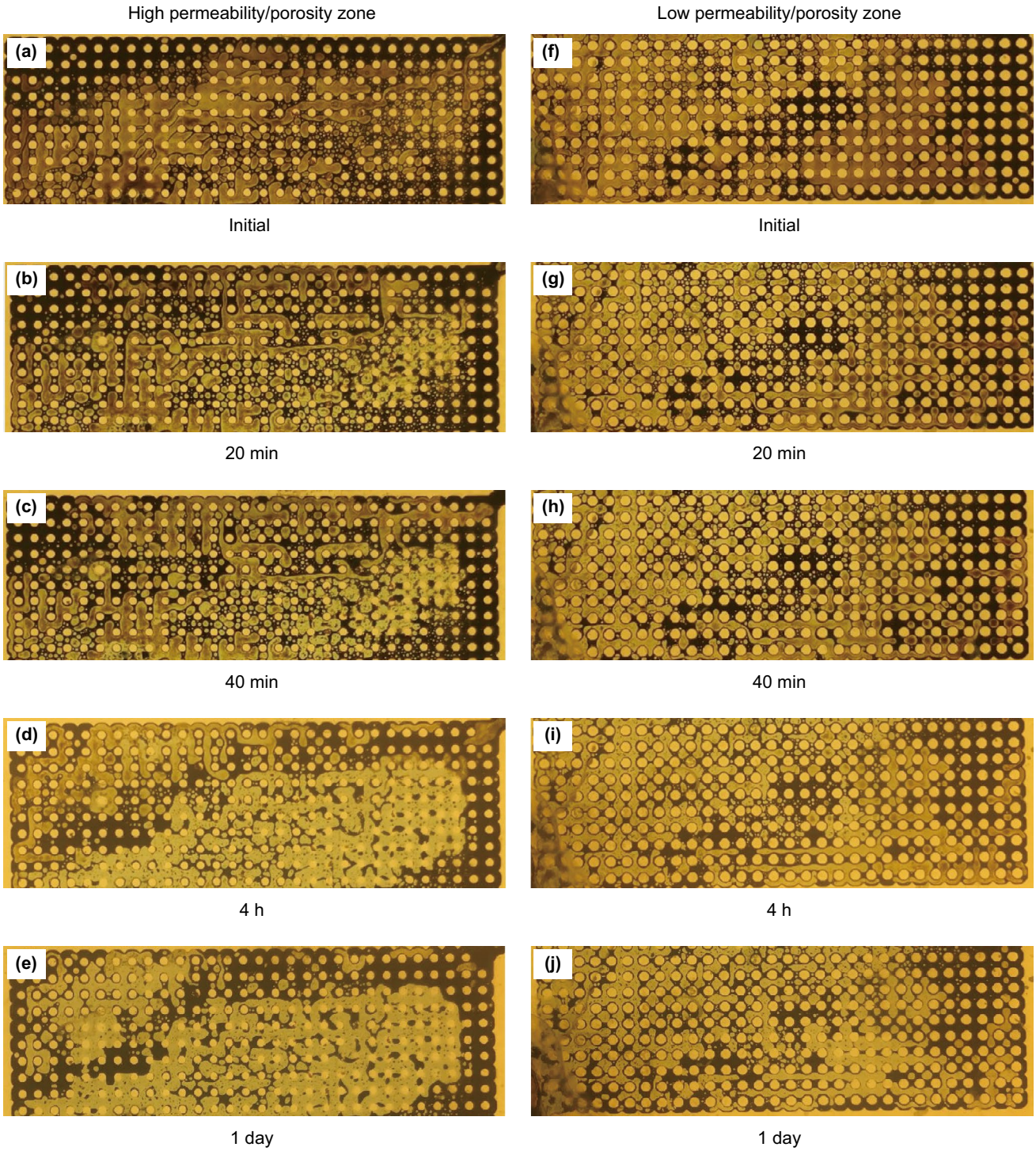

Fig. 12 Distribution of the fluids in different regions of the micromodel versus time, after injection of Na_2CO_3. For more details, see the electronic supplementary video 5. **a–e** High permeability/porosity zone, and **f–j** low permeability/porosity zone

(Na_2CO_3, and $MgSO_4$ solutions) and in different micromodel regions. Since in the case of Na_2CO_3 flooding, the Marangoni and capillary forces are positive and resistive to flow, respectively, and then larger values of this number indicate higher flow potential in the investigated zone. In other words, the higher the surface tension gradient, and the lesser the IFT would lead to easier alkaline flow and more oil sweeping. Table 9 compares the magnitude of ψ for both alkaline flooding cases which shows that the value of ψ for the Na_2CO_3 solution is more than three orders of magnitude

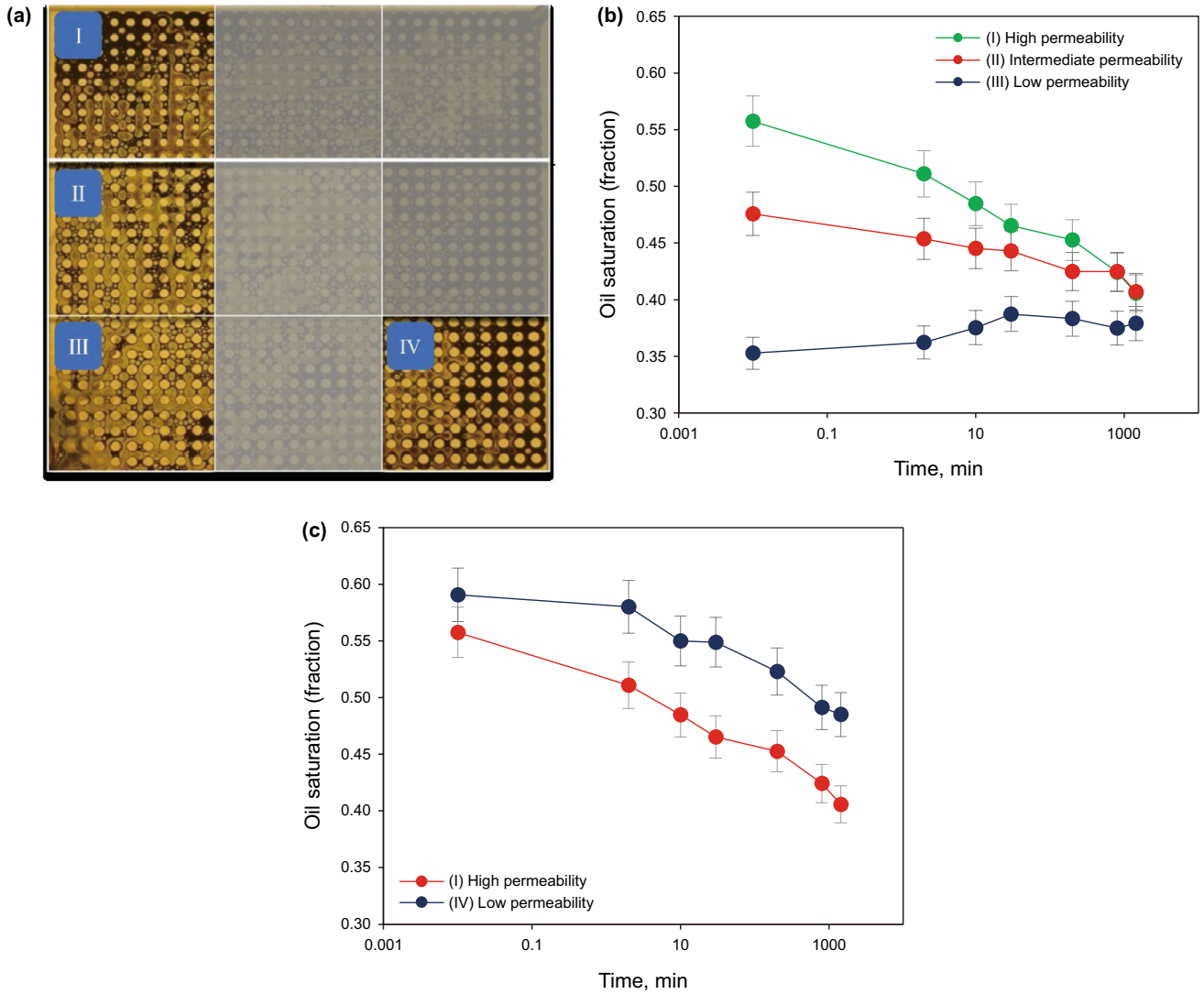

Fig. 13 Oil saturation obtained using image processing of the micromodel experiments for Na_2CO_3 flooding. **a** Selected zones with different pore sizes and oil saturations. **b** Curves of oil saturation in the regions I, II, and III of the micromodel versus time. **c** Trend of oil saturation in unswept regions (I and IV) of the micromodel versus time

Table 9 The Marangoni/capillary force dimensionless number (ψ) for different alkalines

Micromodel region	Pore radius, μm	ψ	
		Na_2CO_3 flooding	$MgSO_4$ flooding
High permeability	200	$>3.01\times10^{2}$	7.89×10^{-2}
Intermediate permeability	150	$>2.26\times10^{2}$	5.92×10^{-2}
Low permeability	100	$>1.52\times10^{2}$	3.95×10^{-2}

Notes: The L_m is assumed similar for both Na_2CO_3 and $MgSO_4$ solutions as the height of the micromodel

larger than its value for the $MgSO_4$ solution in a similar micromodel domain. It means that the possibility of occurring movements due to Marangoni convection in the Na_2CO_3 solution flooding is greatly larger than the later one, because of its more powerful driving Marangoni force and less capillary force. The proposed new dimensionless number is also larger for higher permeability zones that indicates the movement is probably more intense in these regions. This

propensity supports the results shown in Fig. 13. Overall, by comparing this number for different alkalines, a justification for the observed phenomenon would be possible in the systems that the extent of other forces such as viscous, gravity and molecular diffusion forces are negligible. The new proposed dimensionless number directly proportions to the rock pore radius in the way that in the rocks with the small pore throats like carbonate rocks or shale rocks the value of capillary force becomes even more imperative.

The magnitude of the proposed dimensionless number also may affect the capillary trapping phenomenon that is a common challenge in heterogeneous porous spaces. An important feature of the Marangoni effect is that due to the direction of generated stresses along with the interface, its direction is usually perpendicular to the direction of front flow which causes better mixing of phases (Park et al. 2020). This makes the injected fluid to flow through the unswept zones where is regularly bypassed by the injection front or left behind due to capillary trapping. This conclusion can be found in Fig. 13 where the oil saturation in the zones with higher oil saturation (unswept zones) experienced more changes. Overall, it can also be deduced the role of Marangoni force needs more attention in porous media, especially in sandstones where the pore sizes are large. This effect would be more noticeable where the viscous forces are negligible, like points where the injection is stopped or where the oil-saturated region is not washed due to the heterogeneities of the rock. It should be noted that even in the cases where other forces such as viscous and capillary forces are active, the presence of Marangoni effect may increase the microscopic efficiency of flooding process by deviating the front of the solvent to the left-behind zones. On the other hand, the presence of these dynamic effects exaggerates the Marangoni convection by mixing of solvents with different concentrations and in situ aqueous phases. In these cases, the presence of these forces makes the flow process more complicated. Finally, creating an ultra-low IFT multiphase flow condition activates the Marangoni convection mechanism along with other mechanisms such as a near-miscible flow that can be highly effective for increased microscopic displacement efficiency of the injection process.

5 Conclusions

In this study, the functionality of solutal Marangoni convection for improving oil recovery in comparison with other mechanisms is characterized in different static and dynamic tests by two different alkalines (Na_2CO_3 and $MgSO_4$). The results obtained in the static tests showed that

- Using Na_2CO_3 led to the fast spreading of oil droplets, however, the spreading using $MgSO_4$ is very slow. The results can be interpreted due to differences in the IFT values observed in the two systems.
- Static tests show that in the case of Na_2CO_3 flooding, the formation of the emulsions becomes more intense due to lower interfacial tension and to more interfacial disturbances (Marangoni convection).

Also, the observations from dynamic tests revealed that

- The Marangoni movements in Na_2CO_3 flooding scenario lead to more movements of the injected chemicals toward the less swept zones resulting in improved oil recovery.
- The observations reveal that Marangoni disturbances are more likely in the zones with larger pores due to more fluid/fluid interface areas and lower capillary forces.
- In the micromodel tests, the dimensionless analysis shows that the viscous, gravity and diffusion forces are negligible in the observed movements and other forces like capillary and Marangoni are needed to be considered.
- The condition for activation of Marangoni convection is introducing an ultra-low IFT condition to a system with a high initial IFT. At this condition, the probability of occurrence of IFT gradient is considerable. Also, low capillary entrapment force condition can be helpful.
- A new dimensionless number as the ratio of the Marangoni to capillary forces is proposed which foresees the multiphase behaviour of fluids in the places where the regular viscous effects do not drain the available oil ganglia by increasing the mixing of phases available in the investigated zone.
- In EOR processes where the main mechanism is IFT reduction, the possibility of occurrence of Marangoni convection needs to be taken into consideration.
- In places where viscous force is negligible, the main dominant forces are the capillary and Marangoni forces and the competition between these forces should be considered.
- In the presence of the viscous effects, activation of Marangoni convection may improve microscopic efficiency of the flooding process by deviating the flow to unswept regions. Also, the viscous effects may improve the Marangoni convection by increasing the mixing of components.

Acknowledgements The authors would like to thank the financial and scientific supports from EOR Research Centre of Shiraz University and the Reservoir Modelling and Simulation Centre (RMSC).

References

Abbasi J, Riazi M, Ghaedi M, Mirzaei-Paiaman A. Modified shape factor incorporating gravity effects for scaling countercurrent imbibition. J Pet Sci Eng. 2017;150:108–14. https://doi.org/10.1016/j.petrol.2016.11.037.

Abolhosseini P, Khosravi M, Rostami B, Masoudi M. Influence of thermal Marangoni convection on the recovery of bypassed oil during immiscible injection. J Pet Sci Eng. 2018;164:196–205. https://doi.org/10.1016/j.petrol.2018.01.060.

Alizadeh M, Rostami B, Khosravi M. Numerical analysis of solutal marangoni convections in porous media. Can J Chem Eng. 2014;92(11):1999–2009. https://doi.org/10.1002/cjce.22016.

Alnoush W, Sayed A, Alyafei N. Optimization of contact angle and interfacial tension measurements for fluid/rock systems at ambient conditions. MethodsX. 2019;6:1706–15. https://doi.org/10.1016/j.mex.2019.07.009.

Baroud CN. Marangoni Convection BT - Encyclopedia of Microfluidics and Nanofluidics. In: Li D, editor. Boston, MA: Springer US; 2013. p. 1–8. https://doi.org/10.1007/978-3-642-27758-0_852-4

Blunt MJ. Multiphase flow in permeable media. Cambridge: Cambridge University Press; 2017.

Castor TP, Somerton WH. Interfacial instabilities in porous media. In: SPE California Regional Meeting. Society of Petroleum Engineers; 1977. https://doi.org/10.2118/6516-MS

Clowes GHA. Protoplasmic equilibrium. J Phys Chem. 1916;20:407–51.

D'Aubeterre A, Da Silva R, Aguilera ME. Experimental study on Marangoni effect induced by heat and mass transfer. Int Commun Heat Mass Transf. 2005;32:677–84. https://doi.org/10.1016/j.icheatmasstransfer.2004.06.012.

Dandekar AY. Petroleum reservoir rock and fluid properties. Boca Raton: CRC Press; 2013.

Davis T, Sigmon K. MATLAB Primer, Seventh Edition. 2004. https://www.crcnetbase.com/doi/book/10.1201/9781420034950.

Debbabi Y, Jackson MD, Hampson GJ, Fitch PJR, Salinas P. Viscous crossflow in layered porous media. Transp Porous Media. 2017a;117:281–309. https://doi.org/10.1007/s11242-017-0834-z.

Debbabi Y, Jackson MD, Hampson GJ, Salinas P. Capillary heterogeneity trapping and crossflow in layered porous media. Transp Porous Media. 2017b;120:183–206. https://doi.org/10.1007/s11242-017-0915-z.

Dong W, Selvadurai APS. Image processing technique for determining the concentration of a chemical in a fluid-saturated porous medium. Geotech Test J. 2006;29:385–91. https://doi.org/10.1520/GTJ100024.

Gong L. Development and applications of the ABEEM fluctuating charge molecular force field in the ion-containing systems. Sci China Chem. 2012;55:2471–84. https://doi.org/10.1007/s11426-012-4787-3.

Gong H, Li Y, Dong M, Ma S, Liu W. Effect of wettability alteration on enhanced heavy oil recovery by alkaline flooding. Colloids Surf A Physicochem Eng Asp. 2016;488:28–35. https://doi.org/10.1016/j.colsurfa.2015.09.042.

Gong H, Li Y, Dong M, Zhu T, Yu L. Enhanced heavy oil recovery by organic alkali combinational flooding solutions. J Dispers Sci Technol. 2017;38:551–7. https://doi.org/10.1080/01932691.2016.1181553.

Herring AL, Andersson L, Schlüter S, Sheppard A, Wildenschild D. Efficiently engineering pore-scale processes: the role of force dominance and topology during nonwetting phase trapping in porous media. Adv Water Resour. 2015;79:91–102. https://doi.org/10.1016/j.advwatres.2015.02.005.

Iervolino M, Pascal J-P, Vacca A. Thermocapillary instabilities of a shear–thinning fluid falling over a porous layer. J Nonnewton Fluid Mech. 2019;270:36–50. https://doi.org/10.1016/j.jnnfm.2019.06.011.

Kazemzadeh Y, Eshraghi SE, Kazemi K, Sourani S, Mehrabi M, Ahmadi Y. Behavior of asphaltene adsorption onto the metal oxide nanoparticle surface and its effect on heavy oil recovery. Ind Eng Chem Res. 2015;54(1):233–9. https://doi.org/10.1021/ie503797g.

Khosravi M, Rostami B, Emadi M, Roayaei E. Marangoni flow: an unknown mechanism for oil recovery during near-miscible CO2 injection. J Pet Sci Eng. 2015;125:263–8. https://doi.org/10.1016/j.petrol.2014.11.030.

Kim H, Muller K, Shardt O, Afkhami S, Stone HA. Solutal Marangoni flows of miscible liquids drive transport without surface contamination. Nat Phys. 2017. https://doi.org/10.1038/NPHYS4214.

Liu S, Zhang D, Yan W, Puerto M, Hirasaki GJ, Miller CA. Favorable attributes of alkaline-surfactant-polymer flooding. SPE J. 2008;13:5–16. https://doi.org/10.2118/99744-PA.

Lyford PA, Pratt HRC, Grieser F, Shallcross DC. The Marangoni effect and enhanced oil recovery: Part 1. Porous media studies. Can J Chem Eng. 1998;76(2):167–74. https://doi.org/10.1002/cjce.5450760202.

Lyford PA, Shallcross DC, Pratt HRC, Grieser F. The Marangoni effect and enhanced oil recovery Part 2. Interfacial tension and drop instability. Can J Chem Eng. 1998;76:175–82. https://doi.org/10.1002/cjce.5450760203.

Mahdavi E, Zebarjad FS. Screening criteria of enhanced oil recovery methods fundamentals of enhanced oil and gas recovery from conventional and unconventional reservoirs. Amsterdam: Elsevier; 2018

Masoudi M, Khosravi M, Rostami B, Abolhosseini P. Effect of Bénard-Marangoni flow on the bypassed oil recovery: Micromodel study. J Pet Sci Eng. 2019;178:1067–78. https://doi.org/10.1016/j.petrol.2019.03.064.

Mohammadi H, Delshad M, Pope GA. Mechanistic modeling of alkaline/surfactant/polymer floods. SPE Reserv Eval Eng. 2009;12:518–27. https://doi.org/10.2118/110212-PA.

Nagumo R, Takaba H, Nakao S. High-accuracy estimation of 'slow'' molecular diffusion rates in zeolite nanopores based on free energy calculations at an ultrahigh temperature. J Phys Chem C. 2008;112:2805–11. https://doi.org/10.1021/jp073250b.

Olajire AA. Review of ASP EOR (alkaline surfactant polymer enhanced oil recovery) technology in the petroleum industry: Prospects and challenges. Energy. 2014;77:963–82. https://doi.org/10.1016/j.energy.2014.09.005.(2014).

Park J, Ryu J, Sung HJ, Kim H. Control of solutal Marangoni-driven vortical flows and enhancement of mixing efficiency. J Colloid Interface Sci. 2020;561:408–15. https://doi.org/10.1016/j.jcis.2019.11.006.

Paul A, Laurila T, Vuorinen V, Divinski SV. Thermodynamics diffusion and the kirkendall effect in solids. Berlin: Springer; 2014. p. 115–139.

Pratt HRC. Marangoni flooding with water drives: a novel method for EOR? In: SPE Asia-Pacific Conference, Perth. Australia; 1991. https://doi.org/10.2118/22982-MS

Ramírez-Muñoz J, Galicia-Nequiz OG, Baz-Rodríguez S, Colín-Luna JA, Martínez-Delgadillo SA, Puebla H. The effects of surfactants on the drag of a bubble. Procedia Eng. 2012;42:1840–8. https://doi.org/10.1016/j.proeng.2012.07.579.

Roman S, Soulaine C, AlSaud MA, Kovscek A, Tchelepi H. Particle velocimetry analysis of immiscible two-phase flow in micromodels. Adv Water Resour. 2016;95:199–21111. https://doi.org/10.1016/j.advwatres.2015.08.015.

Sakai T, Kamogawa K, Nishiyama K, Sakai H, Abe M. Molecular diffusion of oil/water emulsions in surfactant-free conditions. Langmuir. 2002;18:1985–90. https://doi.org/10.1021/la0111248.

Schmid KS, Geiger S, Sorbie KS. Analytical solutions for co and counter-current imbibition of sorbing, dispersive solutes in immiscible two-phase flow. Comput Geosci. 2012;16:351–66. https://doi.org/10.1007/s10596-012-9282-6.

Schmitt M, Stark H. Marangoni flow at droplet interfaces: Three-dimensional solution and applications. Phys Fluids. 2016;28:12106. https://doi.org/10.1063/1.4939212.

Sheng J. Modern chemical enhanced oil recovery: theory and practice. Houston: Gulf Professional Publishing; 2010.

Sheng JJ. Critical review of alkaline-polymer flooding. J Pet Explor Prod Technol. 2017;7:147–53. https://doi.org/10.1007/s13202-016-0239-5.

Stebe KJ, Barthès-Biesel D. Marangoni effects of adsorption—desorption controlled surfactants on the leading end of an infinitely long bubble in a capillary. J Fluid Mech. 1995;286:25–48. https://doi.org/10.1017/S0022112095000632.

Troian SM, Herbolzheimer E, Safran SA. Model for the fingering instability of spreading surfactant drops. Phys Rev Lett. 1990;65:333–6. https://doi.org/10.1103/PhysRevLett.65.333.

Velarde MG, Zeytounian RK. Interfacial phenomena and the Marangoni effect. Berlin: Springer; 2002.

Wang S, Zhang Y, Meredith JC, Behrens SH, Tripathi MK, Sahu KC. The dynamics of rising oil-coated bubbles: experiments and simulations. Soft Matter. 2018;14:2724–34.

Yao YL, Liu F, Hu WR. How to determine critical Marangoni number in half floating zone convection. Int J Heat Mass Transf. 1996;39:2539–44. https://doi.org/10.1016/0017-9310(95)00236-7.

Yunyun W, Litao L, Zhengming Y, Weidong L, Xuewei L, Qianhua X. Micro-mechanism of residual oil mobilization by oil-water interface marangoni convection caused by chemical flooding. Electron J Geotech Eng. 2016;21:10559–74.

Zhang D, Du X, Song X, Wang H, Li X, Jiang Y, Wang M. Application of the Marangoni effect in nanoemulsion on improving waterflooding technology for heavy-oil reservoirs. SPE J. 2017;23:831–40. https://doi.org/10.2118/187953-PA.

Zuo L, Zhang C, Falta RW, Benson SM. Micromodel investigations of CO_2 exsolution from carbonated water in sedimentary rocks. Adv Water Resour. 2013;53:188–97. https://doi.org/10.1016/j.advwatres.2012.11.004.